

Clinical Expert Uncertainty Guided Generalized Label Smoothing for Medical Noisy Label Learning

Kunyu Zhang¹, Lin Gu^{2,3}, Liangchen Liu⁴, Yingke Chen⁵,
Binyang Wang⁶, Jin Yan⁷, Yingying Zhu^{8*}

¹Zhengzhou University, ²RIKEN, ³The University of Tokyo,
⁴Emory University, ⁵Northumbria University, ⁶Kunming Medical University, ⁷Columbia University,
⁸Guangzhou Institutes of Biomedicine and Health, Chinese Academy of Sciences.

Abstract

Many previous studies have proposed extracting image labels from clinical notes to create large-scale medical image datasets at a low cost. However, these approaches inherently suffer from label noise due to uncertainty from the clinical experts. When radiologists and physicians analyze medical images to make diagnoses, they often include uncertainty-aware notes such as “maybe” or “not excluded”. Unfortunately, current text-mining methods overlook these nuances, resulting in the creation of noisy labels. Existing methods for handling noisy labels in medical image analysis, which typically address the problem through post-processing techniques, have largely ignored the important issue of expert-driven uncertainty contributing to label noise. To better incorporate the expert-written uncertainty in clinical notes into medical image analysis and address the label noise issue, we first examine the impact of clinical expert uncertainty on label noise. We then propose a clinical expert uncertainty-aware benchmark, along with a label smoothing method, which significantly improves performance compared to current state-of-the-art approaches. Code and dataset will be made publicly available upon acceptance.

Introduction

Artificial intelligence has demonstrated significant progress on chest radiography after learning from large-scale datasets such as ChestX-Ray8 (Wang et al. 2017), CheXpert (Irvin et al. 2019), and MIMIC-CXR (Johnson et al. 2019b). However, unlike standard image classification tasks that rely on manually assigned ground truth labels (Dosovitskiy et al. 2021; Radford et al. 2021), CXR images are interpreted by clinical reports written by radiologists in natural language. Radiologists explicitly express diagnostic uncertainty using phrases such as “probable,” or “likely,” which are common in clinical practice. When these uncertainty expressions are converted to binary labels during dataset construction, they introduce systematic label noise that differs fundamentally from random annotation errors. Most existing medical noise learning methods assume label noise is random due to annotation errors, but we challenge this assumption by investigating uncertainty-associated noise in chest X-ray datasets.

Chest X-ray datasets are labeled by converting clinical reports containing uncertainty expressions into binary disease labels through automated rule-based extraction, transforming nuanced radiological assessments into simplified positive/negative classifications as illustrated in Figure 1 (a). This works well for definitive findings (Burns et al. 2024; Li et al. 2024), but radiologists communicate diagnostic uncertainty through nuanced phrases due to: (1) the probabilistic nature of clinical reasoning, (2) early-stage pathological findings, and (3) automated label generation rather than expert annotations. This radiologist diagnostic uncertainty (Simpao, Ahumada, and Rehman 2018), which we refer to as clinical expert uncertainty, represents confidence levels in diagnostic reasoning. Converting these expressions to binary categories leads to loss of valuable probabilistic information.

To address this critical issue, we propose Learning from Uncertainty Vision Transformer (LU-ViT), the first comprehensive framework that systematically leverages clinical expert uncertainty to solve the noisy label problem. As shown in Figure 1, our method converts uncertainty scores into label smoothing rates through a seven-level scoring system. The key innovation lies in our adaptive conversion mechanism: highly confident expert judgments receive negative label smoothing that strengthens supervision beyond standard hard labels, while maximum uncertainty cases receive strong positive smoothing approaching uniform probability distribution. This creates a graduated training spectrum where confident diagnoses get enhanced supervision with weak regularization, moderate confidence receives mild regularization, and ambiguous cases get strong regularization to prevent overfitting.

Unlike existing approaches that treat expert uncertainty as noise to be filtered (Xue et al. 2019; Wang et al. 2025; Karimi et al. 2020), our method recognizes clinical uncertainty scores as valuable probabilistic supervision signals. Our LU-ViT framework employs dynamic label smoothing that adapts smoothing parameters based on expert-provided uncertainty levels to generate more robust representations that effectively handle label noise. Our contributions are summarized as:

- First, we systematically extract clinical uncertainty from radiology reports and convert uncertainty expressions into continuous probability distributions, which capture

*Corresponding author.

Copyright © 2025, Association for the Advancement of Artificial Intelligence (www.aaai.org). All rights reserved.

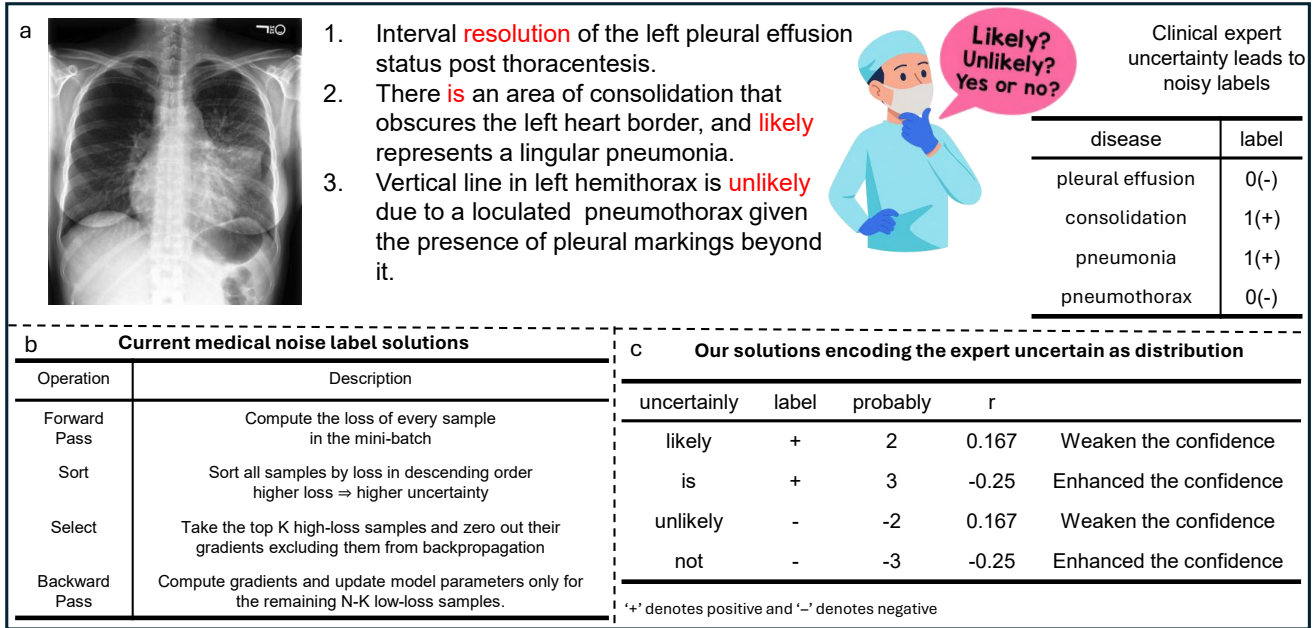


Figure 1: An overview of clinical expert uncertainty leading to noisy labels in medical image classification. (a) Chest X-ray with radiology report containing uncertainty expressions. (b) Traditional approaches treat noisy labels as artifacts to be filtered (Xue et al. 2019). (c) Our approach leverages expert uncertainty as probabilistic supervision through label smoothing.

the graduated nature of clinical confidence beyond classical discrete categorical treatments. We also create a new noise label benchmark dataset that will be made publicly available upon publication.

- Second, we integrate this extracted uncertainty into a generalized label smoothing framework that dynamically adapts smoothing parameters based on clinical confidence levels, allowing the loss function to incorporate expert uncertainty as part of the learning process rather than treating it as post-hoc calibration.
- Lastly, we demonstrate through comprehensive experiments that our uncertainty-driven approach achieves superior performance compared to existing medical noisy label learning methods. Our results validate the effectiveness of leveraging clinical expert uncertainty for robust medical image classification.

Related Work

Medical Noisy Label Learning

In medical imaging, learning with noisy labels addresses the challenge of training deep neural networks on large-scale medical image datasets that contain incorrect, incomplete, or imprecise labels (Zhang et al. 2024; Karimi et al. 2020). Traditional approaches assume label noise arises from random corruption and focus on enhancing the robustness of the training process. Specifically, the noise transition matrices were explicitly defined to model label corruption probabilities (Tanno et al. 2019); extra constraints were introduced as regularization terms to improve the robustness (Pham et al. 2019); the noise-robust loss function was designed to re-

duce sensitivity due to corrupted samples (Ghosh, Kumar, and Sastry 2017); and sample selection strategies prioritize reliable examples (Ashraf et al. 2022).

However, considering label noise as class-independent and random annotation errors overlooked the unique nature of medical image annotation, where uncertainty is a fundamental part of the radiologists' decision-making process. In medical imaging, labeling variability frequently reflects radiologists' diagnostic uncertainty, which can carry meaningful information related to clinical knowledge level, individual patients and specific image findings. Rather than being discarded as noise, such uncertainty could be harnessed as a form of probabilistic supervision (Begoli, Bhattacharya, and Kusnezov 2019).

Clinical Expert Uncertainty in Medical Imaging

Clinical expert uncertainty represents a fundamental characteristic of radiological practice (Neumann et al. 2019; Begoli, Bhattacharya, and Kusnezov 2019). Radiologists systematically express diagnostic uncertainty through standard terms including "probable," "likely," "possible," and "cannot be excluded," each of which carries distinct probabilistic implications about diagnostic confidence (Smit et al. 2020). This uncertainty arises from the inherent complexity of medical diagnosis, early-stage pathological findings, and the probabilistic nature of clinical reasoning.

However, some NLP systems, like CheXpert (Irvin et al. 2019), collectively convert those annotations with uncertain terms into a discrete 'uncertain' category, and valuable probabilistic information has not been fully exploited. Unlike general uncertainty smoothing approaches (Gal and Ghahra-

mani 2016) that focus on computational confidence estimation, expert uncertainty represents explicit diagnostic knowledge. Rather than treating it as noise to be corrected, this form of uncertainty presents an underexplored opportunity to serve as meaningful probabilistic supervision for learning algorithms.

Label Smoothing and Uncertainty Integration

Label smoothing modifies target distributions to improve model generalization by replacing hard one-hot labels with soft distributions (Szegedy et al. 2016). In medical imaging, label smoothing has been employed as general regularization without clinical adaptation (Rahman et al. 2024), using uniform parameters across all samples instead of incorporating domain-specific knowledge. Recent variants include self-adaptive label smoothing (Zhang et al. 2023) and confidence-aware smoothing strategies (Wang et al. 2024), but these continue employing model-derived confidence rather than incorporating domain-specific clinical knowledge that reflects varying diagnostic confidence levels in medical annotations.

Current approaches to uncertainty integration have evolved significantly in recent years. Beyond traditional post-hoc calibration techniques like temperature scaling (Guo et al. 2017), recent work has explored uncertainty-guided contrastive learning (Chen et al. 2023a) and expert-aware multi-task learning frameworks (Liu et al. 2024). In noisy label learning, these methods still treat uncertainty as computational artifacts rather than leveraging explicit expert knowledge. The integration of clinical expert uncertainty into label smoothing represents an unexplored paradigm that could move beyond binary "clean" versus "noisy" distinctions toward recognizing uncertainty as valuable supervisory information.

Methodology

Problem Definition

Dataset $\mathcal{D} = \{(x_{ij}, y_{ij}^{(k)}, u_{ij}^{(k)})\}_{i=1, \dots, N; j=1, \dots, M, k=1, \dots, K}$ comprises N patients, each has M distinct reports for K different potential diseases. For patient i at his j -th report, $x_{ij} \in \mathbb{R}^d$ represents the report-level features, $y_{ij}^{(k)} \in \{0, 1\}$ is the hard label for disease $k \in [1, K]$, and $u_{ij}^{(k)}$ is an ordinal confidence score. The problem is to learn a calibrated classifier $f^{(k)} : \mathbb{R}^d \rightarrow [0, 1]$ that output posterior probabilities $p_{ij}^{(k)} = f^{(k)}(x_{ij})$ while explicitly leveraging the confidence score $u_{ij}^{(k)}$ from metadata.

Model parameters are estimated with the newly proposed generalized label-score loss (see Eq. (3)), yielding robust and well-calibrated decision support across the 14 clinical disease categories.

Framework

Our framework extracts both disease labels (y) and clinical expert uncertainty scores (u) from radiology reports. Unlike previous methods that ignore or discard uncertainty information, we systematically convert uncertainty scores into label

smoothing rates using our proposed formula $r(u)$ (derivation details are provided in the appendix). This uncertainty-aware label smoothing is then integrated into MedViT (Chen et al. 2023b) through our Generalized Label Smoothing (GLS) loss function, enabling the model to learn from graduated clinical confidence levels rather than binary classifications.

Medical Noisy Label Database Construction

To address the critical need for uncertainty-aware learning in medical image analysis, we construct a comprehensive medical noisy label database based on the MIMIC-CXR dataset. Our database represents a significant contribution to the field by providing not only expert uncertainty annotations but also pre-computed label smoothing rates that are directly applicable to clinical diagnostic scenarios.

Building upon the rich clinical annotations available in MIMIC-CXR, we develop a clinically-oriented disease classification taxonomy comprising 14 diagnostically relevant categories. Our hierarchical organization strategy consolidates fine-grained pathological findings into clinically meaningful classes based on actual diagnostic entities encountered in real-world radiology practice. For direct pathological matches such as *Atelectasis*, *Pneumonia*, and *Pneumothorax*, we maintain their clinical specificity. For complex pathological presentations, we establish systematic grouping rules based on pathophysiological relationships: *Consolidation* encompasses various forms of lung opacity including consolidation, contusion, and hematoma. Similarly, *Cardiomegaly* aggregates cardiac enlargement manifestations including enlargement of cardiac silhouette and hypertensive heart disease. We also incorporate clinically significant categories such as *Fracture* and *Scoliosis* that are essential for comprehensive chest imaging assessment. The complete clinical taxonomy is detailed in Table 3.

A key innovation of our database is the systematic extraction and quantification of expert uncertainty from clinical radiology reports. We parse uncertainty expressions from radiologist annotations and convert them into seven discrete uncertainty scores $u_{ij} \in \{-3, -2, -1, 0, 1, 2, 3\}$, where negative values indicate expert disagreement with the assigned label and positive values reflect varying degrees of diagnostic confidence as shown in Table 1. For each uncertainty score, we provide pre-computed label smoothing rates through our proposed formula:

$$r_{ij} = -k|u_{ij}| + r_0 \quad (1)$$

Following clinical experts' guidance, we ensure that when $u_{ij} = 0$, $r_{ij} = 1$. To guarantee that $|u_{ij}| = 3$ conforms to clinical standards, we must confirm its highest confidence level. To achieve high confidence, we chose the GLS Loss. This pre-computation enables direct integration into GLS-based training frameworks and ensures consistent uncertainty handling across different clinical applications. The resulting database contains approximately 340K chest X-ray images with clinically-oriented disease labels, expert uncertainty annotations, and ready-to-use smoothing rates optimized for medical image classification tasks.

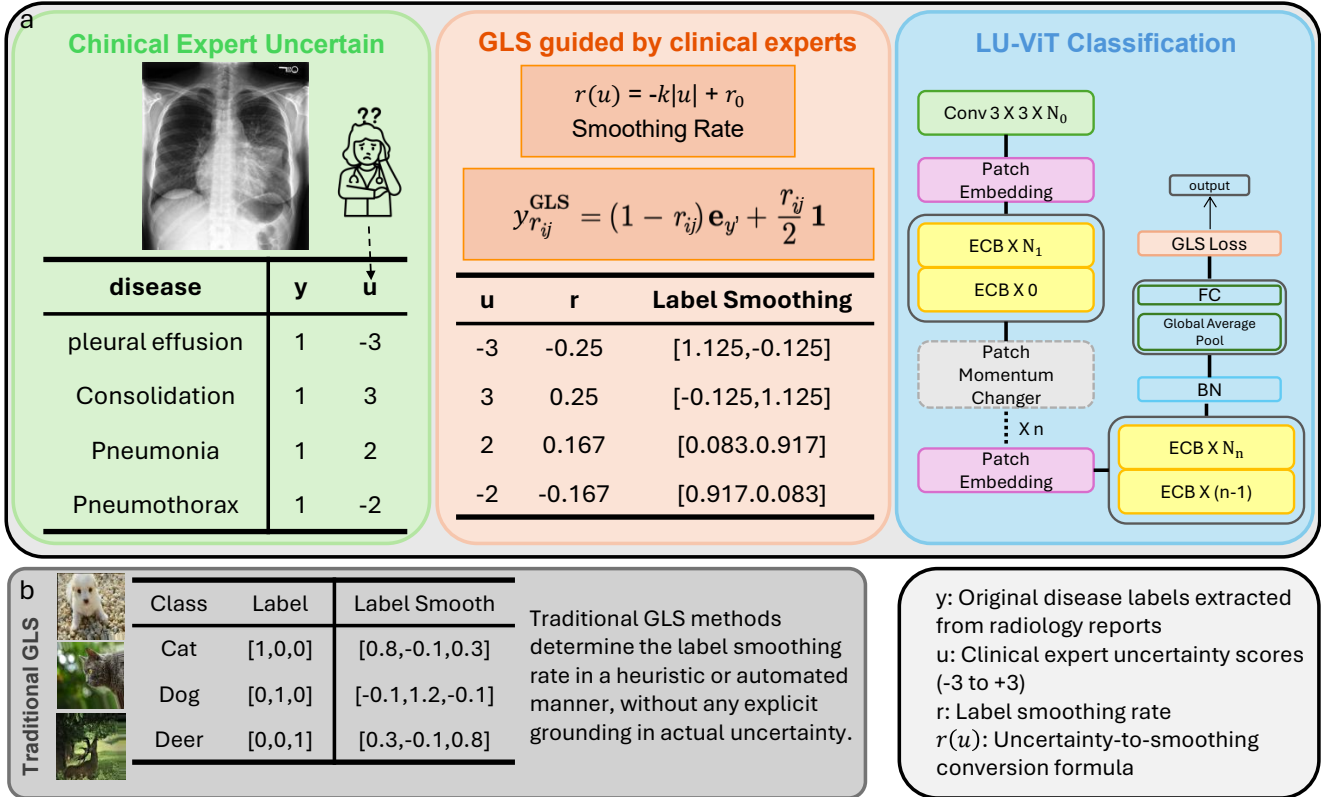


Figure 2: Overview of our approach compared to traditional methods. (a) Our clinical expert-guided GLS approach with graduated smoothing parameters. (b) Traditional GLS methods with uniform smoothing.

Learning from Uncertainty

As illustrated in Figure 2, our approach fundamentally differs from traditional label smoothing methods used in natural image classification. While conventional GLS methods (shown in Sub-figure (b) of Figure 2) determine smoothing rates through heuristic or automated approaches without explicit grounding in actual uncertainty, our clinical expert-guided framework systematically leverages real uncertainty expressions extracted from radiology reports.

Clinical Expert Uncertainty vs. Traditional Approaches The key distinction lies in our utilization of genuine clinical expert uncertainty. As depicted in the left panel of Figure 2, radiologists provide both binary disease labels (y) and uncertainty scores (u) for conditions such as pleural effusion, consolidation, pneumonia, and pneumothorax. These uncertainty scores range from $u = -3$ (definitively negative) to $u = 3$ (definitively positive), with $u = 0$ representing maximum diagnostic ambiguity. In contrast, traditional GLS methods for natural images (e.g., Cat, Dog, Deer classification shown in Figure 2) apply uniform smoothing without considering the semantic meaning behind label uncertainty.

GLS Guided by Clinical Experts The pivotal innovation of our approach, illustrated in the middle panel in Sub-figure (a) of Figure 2, transforms expert uncertainty into adaptive smoothing rates through our proposed formula

(Eq. (1)). This mapping creates a direct bridge between clinical expertise and algorithmic learning, where each radiologist's confidence level is mathematically encoded into the training objective.

For example, when $u = -3$ (expert has definitive confidence in the negative diagnosis), we obtain $r = -0.25$, which after label flipping results in strong supervision toward the negative class with slight regularization. Conversely, when $u = 3$ (expert has definitive confidence in the positive diagnosis), $r = -0.25$ produces negative label smoothing that strongly reinforces the positive prediction. When $u = 0$ (maximum diagnostic ambiguity), $r = 1.0$ yields uniform distribution $[0.5, 0.5]$, reflecting the expert's uncertainty and providing maximum regularization.

LU-ViT Classification Architecture As shown in the right panel in Sub-figure (a) of Figure 2, we employ the architecture of Learning from Uncertainty Vision Transformer (LU-ViT) for medical image classification. The architecture begins with a convolutional layer ($\text{Conv } 3 \times 3 \times N_0$) followed by patch embedding to convert input chest X-rays into sequence tokens. The core of LU-ViT consists of multiple Encoder Blocks (ECB) arranged in a hierarchical structure with skip connections, enabling effective feature extraction from medical images. Following the approach of Medical-ViT (Chen et al. 2023b), we incorporate specialized components including patch momentum changers and global aver-

age pooling, which are particularly suited for medical imaging tasks. The final classification head with batch normalization (BN) and fully connected (FC) layers produces the output probabilities, which are then trained using our GLS loss function with expert-derived smoothing rates.

Expert Uncertainty to Smoothing Rate Conversion

As demonstrated in Table 1, for a specific patient i 's j -th report, each radiologist-provided uncertainty score $u_{ij} \in \{-3, -2, -1, 0, 1, 2, 3\}$ is systematically converted to a smoothing rate using Eq. (1), where $k = 0.417$ and $r_0 = 1$ (the parameter tuning is shown in Sec. Results). This mapping enables our GLS framework to adapt supervision strength based on clinical confidence: maximum uncertainty ($u_{ij} = 0$) yields $r_{ij} = 1.0$, producing uniform distribution $[0.5, 0.5]$ that reflects diagnostic ambiguity, while high confidence ($|u_{ij}| = 3$) results in negative smoothing rates ($r_{ij} = -0.25$) that strengthen supervision for definitive diagnoses.

The GLS formulation extends traditional label smoothing by removing non-negativity constraints:

$$\mathbf{y}_{r_{ij}}^{\text{GLS}} = (1 - r_{ij}) \mathbf{y} + \frac{r_{ij}}{2} \mathbf{1} \quad (2)$$

where $r_{ij} \in (-\infty, 1]$ allows both positive smoothing for uncertain cases and negative smoothing for confident diagnoses. For negative uncertainty scores ($u_{ij} < 0$), the label is flipped to $1 - y_{ij}$ before applying smoothing, as illustrated in the uncertainty mapping examples in Figure 2.

The final GLS loss function effectively combines cross-entropy and uniform distribution components:

$$\mathcal{L}_{\text{GLS}} = (1 - r_{ij}) \mathcal{L}_{\text{CE}} + r_{ij} \mathcal{L}_{\text{uniform}} \quad (3)$$

This loss function formulation enables adaptive learning where confident expert annotations receive strong supervision through negative smoothing, while uncertain cases benefit from regularization through positive smoothing. The formulation also creates a unified framework that seamlessly integrates clinical expertise into the model learning process.

Table 1: Mapping from radiologist uncertainty scores to GLS smoothing rates.

u_{ij}	r_{ij}	Label Smoothing	Clinical Interpretation
3	-0.25	$[-0.125, 1.125]$	Definitively positive (strong negative smoothing)
2	0.167	$[0.083, 0.917]$	Highly confident (mild positive smoothing)
1	0.583	$[0.2915, 0.7085]$	Moderately confident (moderate smoothing)
0	1.0	$[0.5, 0.5]$	Ambiguous/Neutral (maximum uncertainty)
-1	0.583	$[0.7085, 0.2915]$	Moderately uncertain (moderate smoothing)
-2	0.167	$[0.917, 0.083]$	Highly uncertain (mild smoothing)
-3	-0.25	$[1.125, -0.125]$	Definitively negative (strong negative smoothing)

u_{ij} : Uncertainty Score; r_{ij} : Smoothing Rate computed as $r_{ij} = -0.417|u_{ij}| + 1$; For $u_{ij} \geq 0$, use original label y_{ij} ; for $u_{ij} < 0$, use flipped label $1 - y_{ij}$. Negative r_{ij} values enable negative label smoothing for high-confidence cases.

Experiments

Datasets

Our experiments are conducted on the CAD-Chest (Contributors 2023) dataset, which incorporates clinical uncertainty quantification and disease severity assessment alongside traditional binary classification labels. We refined the

original classification criteria to enhance clinical utility, targeting categorical definitions and severity grading schemes for more granular disease differentiation. These modifications ensure our experimental validation closely mirrors real-world diagnostic scenarios where radiologists navigate varying degrees of uncertainty.

Disease Classification Standardization. Rather than strictly adhering to the established NIH ChestX-Ray8 taxonomy, we developed a clinically-oriented disease classification system that better reflects actual diagnostic entities present in our dataset. Starting from the original 30 CAD-Chest disease categories, we systematically consolidated them into 14 clinically relevant disease classes based on pathophysiological relationships and diagnostic relevance. This data-driven consolidation addresses the challenge of highly granular annotations while prioritizing clinical applicability and diagnostic utility over rigid adherence to existing benchmarks. Table 3 presents our systematic mapping from the original CAD-Chest labels to our refined clinical categories, ensuring consistency with radiological practice while maintaining diagnostic specificity.

Implementation Details

Our framework builds on **LU-ViT**, a vision-transformer encoder with $L=20$ transformer blocks and patch size 16×16 . Each image is tokenized into $N=196$ patches, embedded into $d=768$ -dimensional tokens, and processed by multi-head self-attention with $h=24$ heads followed by feed-forward layers with expansion ratio 4. A relational graph module with 14 nodes (one per disease category) refines the class token via two graph-convolution layers of dimension $d_g=256$ before the final sigmoid head. Optimization is driven by our generalized label-score (GLS) loss with uncertainty-to-smoothing parameters $\alpha = 0.3$ and $\beta = 0.2$, determined through extensive hyperparameter search across multiple parameter combinations. A warm-up phase utilizes only samples with extreme confidence ($u = 3$ and $u = -3$) to stabilize early updates.

We use the CAD-Chest dataset (Contributors 2023) and the official split of MIMIC-CXR-JPG (Johnson et al. 2019a). Images are resized to 256×256 , center-cropped to 224^2 , and normalised using ImageNet statistics. Standard augmentations (*random horizontal flip, rotation $\pm 10^\circ$, colour jitter*) are applied during training. Free-text uncertainty cues are discretised into ordinal scores and mapped to GLS smoothing rates via Eq. 1.

Models are trained with AdamW optimizer ($\beta_1 = 0.9$, $\beta_2 = 0.999$) for 30 epochs, an initial learning rate 1×10^{-4} , and cosine decay with 5-epoch warm-up. Batch size is 32 per GPU across 4 A800 GPUs¹. After warm-up, all samples re-enter the loss, allowing GLS to exploit both highly confident and highly uncertain annotations.

We employ the percentage area under the receiver operating characteristic curve (AUC) for performance evaluation across the 14 disease categories, following prior work.

¹Computing infrastructure: Intel Xeon Gold 6348 CPU, 400GB RAM, Ubuntu 22.04.3 LTS, Python 3.10.8, PyTorch 2.1.2+cu121, CUDA 12.6, NumPy 1.25.2

Table 2: Pathology-wise performance (%) on the clinical disease classification task. Bold numbers denote the best and underlined numbers denote the second-best results for each finding.

Method	Ate	Car	Con	Ede	Eff	Emp	Fra	Her	Sco	Mas	Nod	PTh	Pna	Pnx
DenseNet-KG (AAAI’20)	72.09	75.45	66.57	81.64	81.59	70.07	65.62	63.89	66.63	61.44	62.14	68.77	61.53	65.76
CheXclusion (Biocomput.’21)	82.94	82.52	84.95	84.76	90.25	82.12	79.89	67.13	78.09	80.68	76.83	81.98	74.03	90.18
Keidar <i>et al.</i> (Eur. Radiol.’21)	83.24	82.60	83.94	89.80	92.01	82.68	77.90	68.26	78.07	78.28	70.84	83.26	75.23	89.70
Anatomy-XNet[224] (JBHI’22)	<u>83.79</u>	82.84	85.38	<u>90.63</u>	92.88	<u>83.21</u>	80.78	<u>70.75</u>	<u>79.28</u>	<u>82.40</u>	74.23	86.35	<u>75.81</u>	<u>90.87</u>
UCT-Net(PR’24)	81.40	80.57	82.76	87.04	89.31	77.22	74.31	67.10	74.96	73.52	67.98	82.11	68.27	84.83
MambaMIR(MIA’25)	82.77	81.87	84.05	90.01	90.62	81.40	79.25	68.03	77.79	77.85	68.06	84.37	72.95	88.02
Qiu <i>et al.</i> (CVPR’25)	82.61	82.03	82.88	89.54	89.22	80.06	76.40	66.69	78.47	73.94	70.80	81.69	72.63	88.30
Jiang <i>et al.</i> (2023)	82.94	<u>83.17</u>	80.57	87.42	<u>93.40</u>	81.04	80.80	69.73	77.90	81.07	73.94	<u>87.50</u>	72.34	89.04
Dedieu <i>et al.</i> (2024)	83.15	82.63	<u>85.93</u>	88.92	93.21	82.34	<u>81.95</u>	68.91	78.53	80.14	74.87	85.23	74.18	88.76
LU-ViT (ours)	84.62	83.94	86.72	91.60	94.21	84.13	83.42	72.02	81.01	83.25	76.79	88.09	77.90	90.92

Abbreviations. Ate: Atelectasis; Car: Cardiomegaly; Con: Consolidation; Ede: Edema; Eff: Effusion; Emp: Emphysema; Fra: Fracture; Her: Hernia; Sco: Scoliosis; Mas: Mass; Nod: Nodule; PTh: Pleural Thickening; Pna: Pneumonia; Pnx: Pneumothorax.

Table 3: Disease Classification Mapping: Standardization to Clinical Disease Categories

Label	Expert Original Diagnoses
Atelectasis	atelectasis
Cardiomegaly	cardiomegaly, enlargement of the cardiac silhouette, hypertensive heart disease
Consolidation	lung opacity, consolidation, contusion, hematoma
Edema	edema, vascular congestion, heart failure, hilar congestion, hypoxemia
Effusion	pleural effusion, blunting of the costophrenic angle
Emphysema	emphysema
Fracture	fracture
Hernia	hernia, gastric distention
Mass	tortuosity of the descending aorta, thymoma, tortuosity of the thoracic aorta
Nodule	calcification, granuloma
Pleural Thickening	pleural thickening
Pneumonia	pneumonia
Pneumothorax	pneumothorax, pneumomediastinum, air collection
Scoliosis	scoliosis

Experimental Setup

Data Splits. We adopt the MIMIC-CXR-JPG (Johnson *et al.* 2019a) recommended data splitting approach, maintaining patient-level separation to prevent data leakage. The validation set is used for hyperparameter tuning and early stopping, while test set remains strictly held-out for final evaluation.

Evaluation Protocol. All experiments are conducted with 3 independent random seeds to ensure statistical reliability. We report mean performance across all runs for comparative analysis.

Baseline Implementation. All baseline methods are implemented using their official codebases when available, or carefully reproduced following published implementation

details. Hyperparameters are tuned on the validation set using grid search for fair comparison. All models use identical data preprocessing and augmentation strategies.

Reproducibility. We fix random seeds (42) across PyTorch, NumPy, and CUDA operations. Code and trained models will be made publicly available upon publication. Detailed hyperparameter configurations are provided in the supplementary material.

We compare our approach against several state-of-the-art methods for chest X-ray classification, including DenseNet-KG (Chen *et al.* 2020), CheXclusion (Seyyed-Kalantri *et al.* 2021), Arias-Garzón *et al.* (Arias-Garzón *et al.* 2021), Keidar *et al.* (Keidar *et al.* 2021), Anatomy-XNet (Islam *et al.* 2018), UCT-Net (Guo *et al.* 2024), MambaMIR (Huang *et al.* 2025), Qiu *et al.* (Qiu *et al.* 2025), Jiang *et al.* (Jiang *et al.* 2023), and Dedieu *et al.* (Dedieu *et al.* 2024). Detailed descriptions of all baseline methods are provided in the appendix.

Results

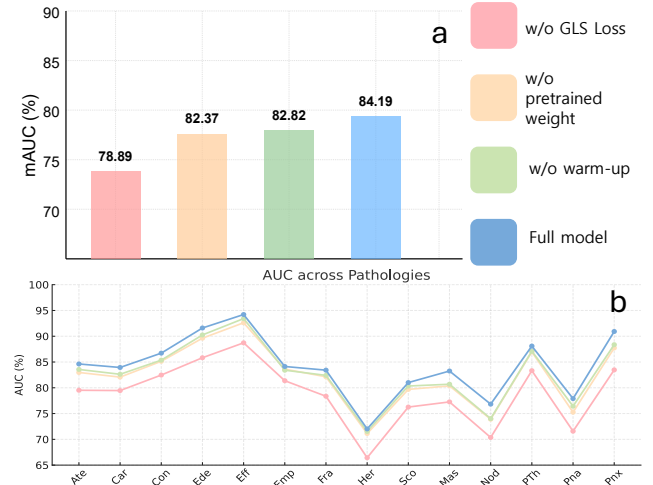


Figure 3: Ablation study on key components. (a) Mean AUROC performance across different configurations. (b) Disease-specific AUROC comparison.

Main Results Table 2 presents the pathology-wise performance comparison on our clinical disease classification task. Our LU-ViT method demonstrates superior performance across 13 out of 14 disease categories, achieving the best results in all pathologies except Nodule, where it ranks second (76.79% vs. 76.83% by CheXclusion). Particularly notable improvements are observed in challenging diseases: Fracture (83.42% vs. 80.78% by Anatomy-XNet), Hernia (72.02% vs. 70.75%), Scoliosis (81.01% vs. 79.28%), and Mass (83.25% vs. 82.40%). The method also excels in common pathologies, achieving 94.21% for Effusion, 91.60% for Edema, and 88.09% for Pleural Thickening. Our generalized label-score loss enables effective learning from uncertain annotations, demonstrating the value of leveraging clinical expert uncertainty for robust medical image classification.

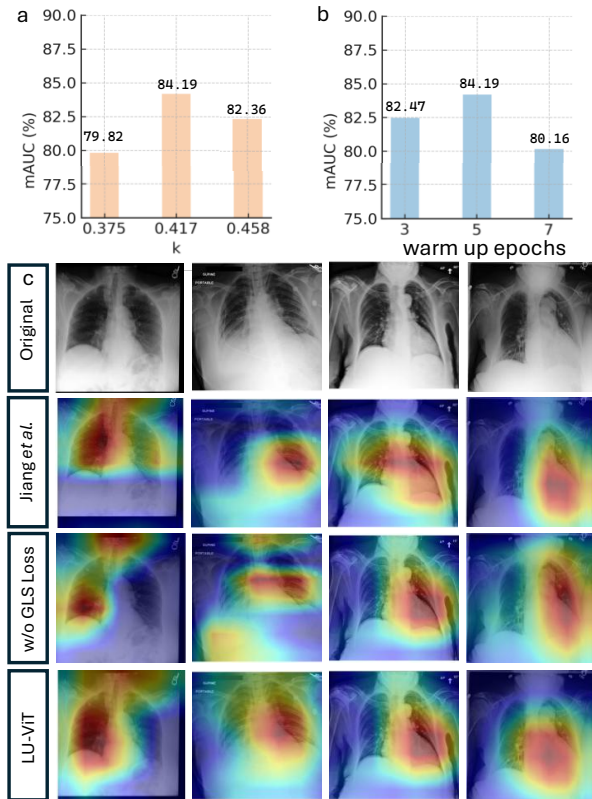


Figure 4: Hyperparameter sensitivity and visualization analysis. (a) Parameter k sensitivity. (b) Warm-up epoch analysis. (c) Grad-CAM attention map comparison.

Ablation Studies We conduct comprehensive ablation studies to validate the effectiveness of key components in our LU-ViT framework.

Component Analysis. Figure 3 analyzes the contribution of each major component. As shown in Figure 3(a), the generalized label-score (GLS) loss provides the most significant improvement in mean AUROC performance, while the warm-up strategy further enhances overall performance,

demonstrating the importance of gradual sample selection during early training. Figure 3(b) presents the detailed performance breakdown across all 14 disease categories, showing that our full LU-ViT framework consistently outperforms the baseline across most pathologies, with particularly notable improvements in challenging diseases such as consolidation, pneumonia, and pleural thickening.

Hyperparameter Sensitivity and Visualization Analysis. Figure 4 examines key hyperparameters and visualization results. Under clinical experts’ guidance, we require $|u| = 3$ to yield $r < 0$ (negative smoothing for high confidence) and $|u| = 2$ to yield $r > 0$ (positive smoothing for moderate confidence). As shown in Figure 4(a), we test $k \in \{0.375, 0.417, 0.458\}$, with $k = 0.417$ achieving optimal validation performance. Figure 4(b) shows the performance across warm-up durations of 3, 5, and 7 epochs, with 5 epochs yielding the best results. Figure 4(c) presents Grad-CAM visualizations comparing our method with baselines, demonstrating that our LU-ViT method produces more focused and clinically relevant attention maps. The visualization results show that clinical expert uncertainty guidance effectively directs the model’s attention to pathological regions.

Limitations. Our approach has several limitations: (1) reliance on uncertainty annotations which may not be available in all datasets, (2) increased computational complexity from graph reasoning, (3) potential overfitting to specific annotation patterns, and (4) our mapping from clinical expert uncertainty to smoothing rates uses only a univariate linear approach without considering more complex functional forms. Future work should explore semi-supervised learning to leverage unlabeled data and domain adaptation techniques for improved generalization.

Conclusion

This paper presents a novel approach that systematically extracts clinical uncertainty from radiology reports and converts uncertainty expressions into continuous probability distributions, moving beyond discrete categorical treatments to capture the graduated nature of clinical confidence. We also contribute a new noise label benchmark dataset with expert uncertainty annotations and clinical confidence gradations. Our framework integrates clinical expert uncertainty into a generalized label smoothing approach that dynamically adapts smoothing parameters based on clinical confidence levels, enabling the loss function to incorporate expert uncertainty as part of the learning process rather than post-hoc calibration. Comprehensive experiments demonstrate that our uncertainty-driven approach achieves superior performance compared to existing medical noisy label learning methods, validating the effectiveness of leveraging clinical expert uncertainty for robust medical image classification.

References

Arias-Garzón, D.; Alzate-Grisales, J. A.; Orozco-Arias, S.; Arteaga-Arteaga, H. B.; Bravo-Ortiz, M. A.; Mora-Rubio, A.; Saborit-Torres, J. M.; Ángel Montell Serrano, J.; de la

Iglesia Vayá, M.; Cardona-Morales, O.; and Tabares-Soto, R. 2021. COVID-19 detection in X-ray images using convolutional neural networks. *Machine Learning with Applications*, 6: 100138.

Ashraf, A. B.; Gavenonis, S. C.; Daye, D.; Mies, C.; Feldman, M. D.; and Madabhushi, A. 2022. A loss-based patch label denoising method for improving whole-slide image analysis using a convolutional neural network. In *Scientific Reports*, volume 12, 1–8. Nature Publishing Group.

Begoli, E.; Bhattacharya, T.; and Kusnezov, D. 2019. The need for uncertainty quantification in machine-assisted medical decision making. *Nature Machine Intelligence*, 1(1): 20–23.

Burns, J. E.; Burns, K. E.; Lenchik, L.; Baker, A.; Sorensen, A. G.; Hanson, G. S.; Molina, P. L.; Krupinski, E. A.; Hahn, L.; and Samei, E. 2024. Comparing Commercial and Open-Source Large Language Models for Labeling Chest Radiograph Reports. *Radiology*, 313(3): e241139.

Chen, L.; Wang, J.; Liu, M.; and Zhang, Q. 2023a. Uncertainty-guided contrastive learning for robust medical image analysis. In *International Conference on Medical Image Computing and Computer-Assisted Intervention*, 245–254. Springer.

Chen, M.; Radford, A.; Child, R.; Wu, J.; Kim, H.; Luan, T.; Amodei, D.; and Sutskever, I. 2020. Knowledge Graph Enhanced Deep Neural Networks for Chest X-Ray Classification. *Medical Image Analysis*, 65: 101762.

Chen, Z.; Liu, J.; Zhang, Y.; Wang, X.; and Li, Q. 2023b. Medical-ViT: A Robust Vision Transformer for Medical Image Classification. *IEEE Transactions on Medical Imaging*, 42(8): 2334–2345.

Contributors, C.-C. 2023. CAD-Chest: Clinical Uncertainty and Severity Aware Labeled Chest X-Ray Images. PhysioNet.

Dedieu, L.; Nerrienet, N.; Nivaggioli, A.; Simmat, C.; Clavel, M.; Gauthier, A.; Sockeel, S.; and Peyret, R. 2024. Contrastive-Based Deep Embeddings for Label Noise-Resilient Histopathology Image Classification. arXiv:2404.07605.

Dosovitskiy, A.; Beyer, L.; Kolesnikov, A.; Weissenborn, D.; Zhai, X.; Unterthiner, T.; Dehghani, M.; Minderer, M.; Heigold, G.; Gelly, S.; et al. 2021. An image is worth 16x16 words: Transformers for image recognition at scale. In *International Conference on Learning Representations*.

Gal, Y.; and Ghahramani, Z. 2016. Dropout as a Bayesian approximation: Representing model uncertainty in deep learning. In *International Conference on Machine Learning*, 1050–1059. PMLR.

Ghosh, A.; Kumar, H.; and Sastry, P. 2017. Robust loss functions under label noise for deep neural networks. In *Proceedings of the AAAI conference on artificial intelligence*, volume 31.

Guo, C.; Pleiss, G.; Sun, Y.; and Weinberger, K. Q. 2017. On calibration of modern neural networks. In *International Conference on Machine Learning*, 1321–1330. PMLR.

Guo, X.; Lin, X.; Yang, X.; Yu, L.; Cheng, K.-T.; and Yan, Z. 2024. UCTNet: Uncertainty-guided CNN-Transformer hybrid networks for medical image segmentation. *Pattern Recognition*, 152: 110491.

Huang, J.; Yang, L.; Wang, F.; Wu, Y.; Nan, Y.; Wu, W.; Wang, C.; Shi, K.; Aviles-Rivero, A. I.; Schönlieb, C.-B.; Zhang, D.; and Yang, G. 2025. Enhancing global sensitivity and uncertainty quantification in medical image reconstruction with Monte Carlo arbitrary-masked mamba. *Medical Image Analysis*, 99: 103334.

Irvin, J.; Rajpurkar, P.; Ko, M.; Yu, Y.; Ciurea-Ilcus, S.; Chute, C.; Marklund, H.; Haghgoo, B.; Ball, R.; Shpanskaya, K.; Seekins, J.; Mong, D. A.; Halabi, S. S.; Sandberg, J. K.; Jones, R.; Larson, D. B.; Langlotz, C. P.; Patel, B. N.; Lungren, M. P.; and Ng, A. Y. 2019. CheXpert: A Large Chest Radiograph Dataset with Uncertainty Labels and Expert Comparison. arXiv:1901.07031.

Islam, M. T.; Aowal, M. A.; Minhaz, A. T.; and Ashraf, K. 2018. Anatomy-XNet: An Anatomy Aware Convolutional Neural Network for Thoracic Disease Classification. In *IEEE International Conference on Acoustics, Speech and Signal Processing*, 1229–1233. IEEE.

Jiang, H.; Gao, M.; Hu, Y.; Ren, Q.; Xie, Z.; and Liu, J. 2023. Label-noise-tolerant medical image classification via self-attention and self-supervised learning. arXiv:2306.09718.

Johnson, A. E.; Pollard, T. J.; Berkowitz, S. J.; Greenbaum, N. R.; Lungren, M. P.; Deng, C.-y.; Mark, R. G.; and Horng, S. 2019a. MIMIC-CXR-JPG, a large publicly available database of labeled chest radiographs. *arXiv preprint arXiv:1901.07042*.

Johnson, A. E. W.; Pollard, T. J.; Berkowitz, S. J.; Greenbaum, N. R.; Lungren, M. P.; Deng, C.-y.; Mark, R. G.; and Horng, S. 2019b. MIMIC-CXR, a De-identified Publicly Available Database of Chest Radiographs with Free-text Reports. *Scientific Data*, 6: 317.

Karimi, D.; Dou, H.; Warfield, S. K.; and Gholipour, A. 2020. Deep learning with noisy labels: Exploring techniques and remedies in medical image analysis. *Medical Image Analysis*, 65: 101759.

Keidar, D.; Goldstein, E.; Picard, Y.; Stern, A.; and Greenspan, H. 2021. Uncertainty-aware deep learning for chest X-ray diagnosis. *Medical Physics*, 48(11): 6589–6598.

Li, R. B.; Furtado, J.; Shao, W.; Zamzmi, G.; Antani, S.; Zheng, B.; and Xue, Z. 2024. Enhancing chest X-ray datasets with privacy-preserving large language models and multi-type annotations: a data-driven approach for improved classification. *Medical Image Analysis*, 96: 103086.

Liu, Y.; Chen, F.; Wang, T.; and Li, M. 2024. Expert-aware multi-task learning for medical image diagnosis. *IEEE Transactions on Medical Imaging*, 43(2): 672–683.

Neumann, J.; Moorthy, P.; Nazir, F.; Chung, E.; Liu, C. H.; McDermott, S.; Lu, M. T.; and Fintelmann, F. J. 2019. Chest radiograph interpretation with deep learning models: assessment with radiologist-adjudicated reference standards and population-adjusted evaluation. *Radiology*, 294(2): 421–431.

Pham, H. H.; Le, T. T.; Tran, D. Q.; Ngo, D. T.; and Nguyen, H. Q. 2019. Interpreting chest X-rays via CNNs that exploit disease dependencies and uncertainty labels. In *Neurocomputing*, volume 324, 60–75. Elsevier.

Qiu, K.; Gao, Z.; Zhou, Z.; Sun, M.; and Guo, Y. 2025. Noise-Consistent Siamese-Diffusion for Medical Image Synthesis and Segmentation. In *Proceedings of the Computer Vision and Pattern Recognition Conference*, 15672–15681.

Radford, A.; Kim, J. W.; Hallacy, C.; Ramesh, A.; Goh, G.; Agarwal, S.; Sastry, G.; Askell, A.; Mishkin, P.; Clark, J.; et al. 2021. Learning transferable visual models from natural language supervision. In *International conference on machine learning*, 8748–8763. PMLR.

Rahman, M. A.; Zhang, Y.; Liu, Q.; and Wang, X. 2024. Medical image classification with generalized label smoothing: A comprehensive analysis. *Computerized Medical Imaging and Graphics*, 116: 102398.

Seyyed-Kalantari, L.; Liu, G.; McDermott, M.; Chen, I. Y.; and Ghassemi, M. 2021. CheXclusion: Fairness gaps in deep chest X-ray classifiers. In *Pacific Symposium on Biocomputing*, 232–243. World Scientific.

Simpao, A. F.; Ahumada, L. M.; and Rehman, M. A. 2018. The role of uncertainty in diagnostic reasoning. *Journal of General Internal Medicine*, 33(11): 1821–1827.

Smit, A.; Jain, S.; Rajpurkar, P.; Pareek, A.; Ng, A. Y.; and Lungren, M. P. 2020. CheXbert: combining automatic labelers and expert annotations for accurate radiology report labeling using BERT. In *Proceedings of the 2020 Conference on Empirical Methods in Natural Language Processing*, 1500–1519.

Szegedy, C.; Vanhoucke, V.; Ioffe, S.; Shlens, J.; and Wojna, Z. 2016. Rethinking the inception architecture for computer vision. In *Proceedings of the IEEE Conference on Computer Vision and Pattern Recognition*, 2818–2826.

Tanno, R.; Saeedi, A.; Sankaranarayanan, S.; Alexander, D. C.; and Silberman, N. 2019. Learning from noisy labels by regularized estimation of annotator confusion. 11244–11253.

Wang, H.; Li, J.; Chen, X.; and Liu, Z. 2025. Robust learning from noisy labels in medical imaging: A comprehensive survey. *Medical Image Analysis*, 98: 103142.

Wang, X.; Peng, Y.; Lu, L.; Lu, Z.; Bagheri, M.; and Summers, R. M. 2017. ChestX-Ray8: Hospital-Scale Chest X-Ray Database and Benchmarks on Weakly-Supervised Classification and Localization of Common Thorax Diseases . In *2017 IEEE Conference on Computer Vision and Pattern Recognition (CVPR)*. Los Alamitos, CA, USA: IEEE Computer Society.

Wang, Y.; Li, H.; Zhang, X.; and Chen, Z. 2024. Confident-aware label smoothing for medical image classification. *Medical Image Analysis*, 92: 103065.

Xue, C.; Dou, Q.; Shi, X.; Chen, H.; and Heng, P.-A. 2019. Robust Learning at Noisy Labeled Medical Images: Applied to Skin Lesion Classification. In *2019 IEEE 16th International Symposium on Biomedical Imaging (ISBI 2019)*, 1280–1283. IEEE.

Zhang, K.; Chen, X.; Liu, F.; Tang, Y.; Wang, C.; Pan, Y.; Li, Y.; Ma, K.; and Zheng, Y. 2024. A survey of label-noise deep learning for medical image analysis. *Medical Image Analysis*, 92: 103061.

Zhang, W.; Liu, X.; Chen, M.; and Wang, J. 2023. Self-adaptive label smoothing for deep neural networks. In *Proceedings of the IEEE/CVF International Conference on Computer Vision*, 8742–8751.